Amplitude Analysis of $D_s^+ \to \pi^+\pi^0\eta$ and First Observation of the W-Annihilation Dominant Decays $D_s^+ \to a_0(980)^+\pi^0$ and $D_s^+ \to a_0(980)^0\pi^+$

M. Ablikim,[1] M. N. Achasov,[10,d] S. Ahmed,[15] M. Albrecht,[4] M. Alekseev,[56a,56c] A. Amoroso,[56a,56c] F. F. An,[1] Q. An,[53,43] J. Z. Bai,[1] Y. Bai,[42] O. Bakina,[27] R. Baldini Ferroli,[23a] Y. Ban,[35] K. Begzsuren,[25] J. V. Bennett,[5] N. Berger,[26] M. Bertani,[23a] D. Bettoni,[24a] F. Bianchi,[56a,56c] E. Boger,[27,b] I. Boyko,[27] R. A. Briere,[5] H. Cai,[58] X. Cai,[1,43] A. Calcaterra,[23a] G. F. Cao,[1,47] N. Cao,[1,47] S. A. Cetin,[46b] J. Chai,[56c] J. F. Chang,[1,43] G. Chelkov,[27,b,c] G. Chen,[1] H. S. Chen,[1,47] J. C. Chen,[1] M. L. Chen,[1,43] S. J. Chen,[33] X. R. Chen,[30] Y. B. Chen,[1,43] W. Cheng,[56c] X. K. Chu,[35] G. Cibinetto,[24a] F. Cossio,[56c] X. F. Cui,[34] H. L. Dai,[1,43] J. P. Dai,[38,h] A. Dbeyssi,[15] D. Dedovich,[27] Z. Y. Deng,[1] A. Denig,[26] I. Denysenko,[27] M. Destefanis,[56a,56c] F. De Mori,[56a,56c] Y. Ding,[31] C. Dong,[34] J. Dong,[1,43] L. Y. Dong,[1,47] M. Y. Dong,[1,43,47] S. X. Du,[61] J. Fang,[1,43] S. S. Fang,[1,47] Y. Fang,[1] R. Farinelli,[24a,24b] L. Fava,[56b,56c] F. Feldbauer,[4] G. Felici,[23a] C. Q. Feng,[53,43] M. Fritsch,[4] C. D. Fu,[1] Q. Gao,[1] X. L. Gao,[53,43] Y. Gao,[45] Y. Gao,[54] Y. G. Gao,[6] Z. Gao,[53,43] B. Garillon,[26] I. Garzia,[24a] A. Gilman,[50] K. Goetzen,[11] L. Gong,[34] W. X. Gong,[1,43] W. Gradl,[26] M. Greco,[56a,56c] M. H. Gu,[1,43] Y. T. Gu,[13] A. Q. Guo,[1] R. P. Guo,[1,47] Y. P. Guo,[26] A. Guskov,[27] S. Han,[58] X. Q. Hao,[16] F. A. Harris,[48] K. L. He,[1,47] X. Q. He,[52] F. H. Heinsius,[4] T. Held,[4] Y. K. Heng,[1,43,47] Y. R. Hou,[47] Z. L. Hou,[1] H. M. Hu,[1,47] J. F. Hu,[38,h] T. Hu,[1,43,47] Y. Hu,[1] G. S. Huang,[53,43] J. S. Huang,[16] X. T. Huang,[37] Z. L. Huang,[31] T. Hussain,[55] W. Ikegami Andersson,[57] W. Imoehl,[22] M. Irshad,[53,43] Q. Ji,[1] Q. P. Ji,[16] X. B. Ji,[1,47] X. L. Ji,[1,43] X. S. Jiang,[1,43,47] X. Y. Jiang,[34] J. B. Jiao,[37] Z. Jiao,[18] D. P. Jin,[1,43,47] S. Jin,[1,47] Y. Jin,[49] T. Johansson,[57] N. Kalantar-Nayestanaki,[29] X. S. Kang,[34] R. Kappert,[29] M. Kavatsyuk,[29] B. C. Ke,[1,l] I. K. Keshk,[4] T. Khan,[53,43] A. Khoukaz,[51] P. Kiese,[26] R. Kiuchi,[1] R. Kliemt,[11] L. Koch,[28] O. B. Kolcu,[46b,f] B. Kopf,[4] M. Kuemmel,[4] M. Kuessner,[4] A. Kupsc,[57] M. Kurth,[1] M. G. Kurth,[1,47] W. Kühn,[28] J. S. Lange,[28] P. Larin,[15] L. Lavezzi,[56c] H. Leithoff,[26] C. Li,[57] Cheng Li,[53,43] D. M. Li,[61] F. Li,[1,43] F. Y. Li,[35] G. Li,[1] H. B. Li,[1,47] H. J. Li,[1,47] J. C. Li,[1] J. W. Li,[41] Jin Li,[36] K. J. Li,[44] Kang Li,[14] Ke Li,[1] L. K. Li,[1] Lei Li,[3] P. L. Li,[53,43] P. R. Li,[47,7] Q. Y. Li,[37] W. D. Li,[1,47] W. G. Li,[1] X. L. Li,[37] X. N. Li,[1,43] X. Q. Li,[34] Z. B. Li,[44] H. Liang,[53,43] H. Liang,[1,47] Y. F. Liang,[40] Y. T. Liang,[28] G. R. Liao,[12] L. Z. Liao,[1,47] J. Libby,[21] C. X. Lin,[44] D. X. Lin,[15] B. Liu,[38,h] B. J. Liu,[1] C. X. Liu,[1] D. Liu,[53,43] D. Y. Liu,[38,h] F. H. Liu,[39] Fang Liu,[1] Feng Liu,[6] H. B. Liu,[13] H. M. Liu,[1,47] Huanhuan Liu,[1] Huihui Liu,[17] J. B. Liu,[53,43] J. Y. Liu,[1,47] K. Y. Liu,[31] Ke Liu,[6] L. D. Liu,[35] Q. Liu,[47] S. B. Liu,[53,43] X. Liu,[30] X. Y. Liu,[1,47] Y. B. Liu,[34] Z. A. Liu,[1,43,47] Zhiqing Liu,[26] Y. F. Long,[35] X. C. Lou,[1,43,47] H. J. Lu,[18] J. G. Lu,[1,43] Y. Lu,[1,*] Y. P. Lu,[1,43] C. L. Luo,[32] M. X. Luo,[60] T. Luo,[9,j] X. L. Luo,[1,43] S. Lusso,[56c] X. R. Lyu,[47] F. C. Ma,[31] H. L. Ma,[1] L. L. Ma,[37] M. M. Ma,[1,47] Q. M. Ma,[1] T. Ma,[1] X. N. Ma,[34] X. Y. Ma,[1,43] Y. M. Ma,[37] F. E. Maas,[15] M. Maggiora,[56a,56c] S. Maldaner,[26] Q. A. Malik,[55] A. Mangoni,[23b] Y. J. Mao,[35] Z. P. Mao,[1] S. Marcello,[56a,56c] Z. X. Meng,[49] J. G. Messchendorp,[29] G. Mezzadri,[24b] J. Min,[1,43] R. E. Mitchell,[22] X. H. Mo,[1,43,47] Y. J. Mo,[6] C. Morales Morales,[15] N. Yu. Muchnoi,[10,d] H. Muramatsu,[50] A. Mustafa,[4] Y. Nefedov,[27] F. Nerling,[11] I. B. Nikolaev,[10,d] Z. Ning,[1,43] S. Nisar,[8] S. L. Niu,[1,43] X. Y. Niu,[1,47] S. L. Olsen,[36,k] Q. Ouyang,[1,43,47] S. Pacetti,[23b] Y. Pan,[53,43] M. Papenbrock,[57] P. Patteri,[23a] M. Pelizaeus,[4] J. Pellegrino,[56a,56c] H. P. Peng,[53,43] K. Peters,[11,g] J. Pettersson,[57] J. L. Ping,[32] R. G. Ping,[1,47] A. Pitka,[4] R. Poling,[50] V. Prasad,[53,43] M. Qi,[33] T. Y. Qi,[2] S. Qian,[1,43] C. F. Qiao,[47] N. Qin,[58] X. S. Qin,[4] Z. H. Qin,[1,43] J. F. Qiu,[1] S. Q. Qu,[34] K. H. Rashid,[55,i] C. F. Redmer,[26] M. Richter,[4] M. Ripka,[26] A. Rivetti,[56c] V. Rodin,[29] M. Rolo,[56c] G. Rong,[1,47] Ch. Rosner,[15] A. Sarantsev,[27,e] M. Savrié,[24b] K. Schoenning,[57] W. Shan,[19] X. Y. Shan,[53,43] M. Shao,[53,43] C. P. Shen,[2] P. X. Shen,[34] X. Y. Shen,[1,47] H. Y. Sheng,[1] X. Shi,[1,43] J. J. Song,[37] X. Y. Song,[1] S. Sosio,[56a,56c] C. Sowa,[4] S. Spataro,[56a,56c] G. X. Sun,[1] J. F. Sun,[16] L. Sun,[58] S. S. Sun,[1,47] X. H. Sun,[1] Y. J. Sun,[53,43] Y. K. Sun,[53,43] Y. Z. Sun,[1] Z. J. Sun,[1,43] Z. T. Sun,[22] Y. T. Tan,[53,43] C. J. Tang,[40] G. Y. Tang,[1] X. Tang,[1] B. Tsednee,[25] I. Uman,[46d] B. Wang,[1] D. Wang,[35] D. Y. Wang,[35] K. Wang,[1,43] L. L. Wang,[1] L. S. Wang,[1] M. Wang,[37] Meng Wang,[1,47] P. Wang,[1] P. L. Wang,[1] W. P. Wang,[53,43] X. L. Wang,[9,j] Y. Wang,[53,43] Y. F. Wang,[1,43,47] Z. Wang,[1,43] Z. G. Wang,[1,43] Z. Y. Wang,[1] Zongyuan Wang,[1,47] T. Weber,[4] D. H. Wei,[12] P. Weidenkaff,[26] S. P. Wen,[1] U. Wiedner,[4] M. Wolke,[57] L. H. Wu,[1] L. J. Wu,[1,47] Z. Wu,[1,43] L. Xia,[53,43] Y. Xia,[20] S. Y. Xiao,[1] Y. J. Xiao,[1,47] Z. J. Xiao,[32] Y. G. Xie,[1,43] Y. H. Xie,[6] X. A. Xiong,[1,47] Q. L. Xiu,[1,43] G. F. Xu,[1] J. J. Xu,[1,47] L. Xu,[1] Q. J. Xu,[14] X. P. Xu,[41] F. Yan,[54] L. Yan,[56a,56c] W. B. Yan,[53,43] W. C. Yan,[2] Y. H. Yan,[20] H. J. Yang,[38,h] H. X. Yang,[1] L. Yang,[58] R. X. Yang,[53,43] Y. H. Yang,[33] Y. X. Yang,[12] Yifan Yang,[1,47] Z. Q. Yang,[20] M. Ye,[1,43] M. H. Ye,[7] J. H. Yin,[1] Z. Y. You,[44] B. X. Yu,[1,43,47] C. X. Yu,[34] J. S. Yu,[30] J. S. Yu,[20] C. Z. Yuan,[1,47] Y. Yuan,[1] A. Yuncu,[46b,a] A. A. Zafar,[55] Y. Zeng,[20] B. X. Zhang,[1] B. Y. Zhang,[1,43] C. C. Zhang,[1] D. H. Zhang,[1] H. H. Zhang,[44] H. Y. Zhang,[1,43] J. Zhang,[1,47] J. L. Zhang,[59] J. Q. Zhang,[4] J. W. Zhang,[1,43,47] J. Y. Zhang,[1] J. Z. Zhang,[1,47] K. Zhang,[1,47] L. Zhang,[45] T. J. Zhang,[38,h] X. Y. Zhang,[37] Y. Zhang,[53,43] Y. H. Zhang,[1,43] Y. T. Zhang,[53,43] Yang Zhang,[1] Yao Zhang,[1] Yi Zhang,[9,j] Z. H. Zhang,[6] Z. P. Zhang,[53]

Z. Y. Zhang,[58] G. Zhao,[1] J. W. Zhao,[1,43] J. Y. Zhao,[1,47] J. Z. Zhao,[1,43] Lei Zhao,[53,43] Ling Zhao,[1] M. G. Zhao,[34] Q. Zhao,[1] S. J. Zhao,[61] T. C. Zhao,[1] Y. B. Zhao,[1,43] Z. G. Zhao,[53,43] A. Zhemchugov,[27,b] B. Zheng,[54] J. P. Zheng,[1,43] Y. H. Zheng,[47] B. Zhong,[32] L. Zhou,[1,43] Q. Zhou,[1,47] X. Zhou,[58] X. K. Zhou,[53,43] X. R. Zhou,[53,43] Xiaoyu Zhou,[20] Xu Zhou,[20] A. N. Zhu,[1,47] J. Zhu,[34] J. Zhu,[44] K. Zhu,[1] K. J. Zhu,[1,43,47] S. H. Zhu,[52] W. J. Zhu,[34] X. L. Zhu,[45] Y. C. Zhu,[53,43] Y. S. Zhu,[1,47] Z. A. Zhu,[1,47] J. Zhuang,[1,43] B. S. Zou,[1] and J. H. Zou[1]

(BESIII Collaboration)

[1]*Institute of High Energy Physics, Beijing 100049, People's Republic of China*
[2]*Beihang University, Beijing 100191, People's Republic of China*
[3]*Beijing Institute of Petrochemical Technology, Beijing 102617, People's Republic of China*
[4]*Bochum Ruhr-University, D-44780 Bochum, Germany*
[5]*Carnegie Mellon University, Pittsburgh, Pennsylvania 15213, USA*
[6]*Central China Normal University, Wuhan 430079, People's Republic of China*
[7]*China Center of Advanced Science and Technology, Beijing 100190, People's Republic of China*
[8]*COMSATS Institute of Information Technology, Lahore, Defence Road, Off Raiwind Road, 54000 Lahore, Pakistan*
[9]*Fudan University, Shanghai 200443, People's Republic of China*
[10]*G.I. Budker Institute of Nuclear Physics SB RAS (BINP), Novosibirsk 630090, Russia*
[11]*GSI Helmholtzcentre for Heavy Ion Research GmbH, D-64291 Darmstadt, Germany*
[12]*Guangxi Normal University, Guilin 541004, People's Republic of China*
[13]*Guangxi University, Nanning 530004, People's Republic of China*
[14]*Hangzhou Normal University, Hangzhou 310036, People's Republic of China*
[15]*Helmholtz Institute Mainz, Johann-Joachim-Becher-Weg 45, D-55099 Mainz, Germany*
[16]*Henan Normal University, Xinxiang 453007, People's Republic of China*
[17]*Henan University of Science and Technology, Luoyang 471003, People's Republic of China*
[18]*Huangshan College, Huangshan 245000, People's Republic of China*
[19]*Hunan Normal University, Changsha 410081, People's Republic of China*
[20]*Hunan University, Changsha 410082, People's Republic of China*
[21]*Indian Institute of Technology Madras, Chennai 600036, India*
[22]*Indiana University, Bloomington, Indiana 47405, USA*
[23a]*INFN Laboratori Nazionali di Frascati, I-00044, Frascati, Italy*
[23b]*INFN and University of Perugia, I-06100, Perugia, Italy*
[24a]*INFN Sezione di Ferrara, I-44122, Ferrara, Italy*
[24b]*University of Ferrara, I-44122, Ferrara, Italy*
[25]*Institute of Physics and Technology, Peace Avenue 54B, Ulaanbaatar 13330, Mongolia*
[26]*Johannes Gutenberg University of Mainz, Johann-Joachim-Becher-Weg 45, D-55099 Mainz, Germany*
[27]*Joint Institute for Nuclear Research, 141980 Dubna, Moscow region, Russia*
[28]*Justus-Liebig-Universitaet Giessen, II. Physikalisches Institut, Heinrich-Buff-Ring 16, D-35392 Giessen, Germany*
[29]*KVI-CART, University of Groningen, NL-9747 AA Groningen, Netherlands*
[30]*Lanzhou University, Lanzhou 730000, People's Republic of China*
[31]*Liaoning University, Shenyang 110036, People's Republic of China*
[32]*Nanjing Normal University, Nanjing 210023, People's Republic of China*
[33]*Nanjing University, Nanjing 210093, People's Republic of China*
[34]*Nankai University, Tianjin 300071, People's Republic of China*
[35]*Peking University, Beijing 100871, People's Republic of China*
[36]*Seoul National University, Seoul, 151-747 Korea*
[37]*Shandong University, Jinan 250100, People's Republic of China*
[38]*Shanghai Jiao Tong University, Shanghai 200240, People's Republic of China*
[39]*Shanxi University, Taiyuan 030006, People's Republic of China*
[40]*Sichuan University, Chengdu 610064, People's Republic of China*
[41]*Soochow University, Suzhou 215006, People's Republic of China*
[42]*Southeast University, Nanjing 211100, People's Republic of China*
[43]*State Key Laboratory of Particle Detection and Electronics, Beijing 100049, Hefei 230026, People's Republic of China*
[44]*Sun Yat-Sen University, Guangzhou 510275, People's Republic of China*
[45]*Tsinghua University, Beijing 100084, People's Republic of China*
[46a]*Ankara University, 06100 Tandogan, Ankara, Turkey*
[46b]*Istanbul Bilgi University, 34060 Eyup, Istanbul, Turkey*
[46c]*Uludag University, 16059 Bursa, Turkey*
[46d]*Near East University, Nicosia, North Cyprus, Mersin 10, Turkey*

[47]University of Chinese Academy of Sciences, Beijing 100049, People's Republic of China
[48]University of Hawaii, Honolulu, Hawaii 96822, USA
[49]University of Jinan, Jinan 250022, People's Republic of China
[50]University of Minnesota, Minneapolis, Minnesota 55455, USA
[51]University of Muenster, Wilhelm-Klemm-Str. 9, 48149 Muenster, Germany
[52]University of Science and Technology Liaoning, Anshan 114051, People's Republic of China
[53]University of Science and Technology of China, Hefei 230026, People's Republic of China
[54]University of South China, Hengyang 421001, People's Republic of China
[55]University of the Punjab, Lahore-54590, Pakistan
[56a]University of Turin, I-10125 Turin, Italy
[56b]University of Eastern Piedmont, I-15121 Alessandria, Italy
[56c]INFN, I-10125 Turin, Italy
[57]Uppsala University, Box 516, SE-75120 Uppsala, Sweden
[58]Wuhan University, Wuhan 430072, People's Republic of China
[59]Xinyang Normal University, Xinyang 464000, People's Republic of China
[60]Zhejiang University, Hangzhou 310027, People's Republic of China
[61]Zhengzhou University, Zhengzhou 450001, People's Republic of China

(Received 14 March 2019; revised manuscript received 25 June 2019; published 12 September 2019)

We present the first amplitude analysis of the decay $D_s^+ \to \pi^+\pi^0\eta$. We use an e^+e^- collision data sample corresponding to an integrated luminosity of 3.19 fb^{-1} collected with the BESIII detector at a center-of-mass energy of 4.178 GeV. We observe for the first time the W-annihilation dominant decays $D_s^+ \to a_0(980)^+\pi^0$ and $D_s^+ \to a_0(980)^0\pi^+$. We measure the absolute branching fraction $\mathcal{B}(D_s^+ \to a_0(980)^{+(0)}\pi^{0(+)}, a_0(980)^{+(0)} \to \pi^{+(0)}\eta) = (1.46 \pm 0.15_{\mathrm{stat}} \pm 0.23_{\mathrm{sys}})\%$, which is larger than the branching fractions of other measured pure W-annihilation decays by at least one order of magnitude. In addition, we measure the branching fraction of $D_s^+ \to \pi^+\pi^0\eta$ with significantly improved precision.

DOI: 10.1103/PhysRevLett.123.112001

The theoretical understanding of the weak decay of charm mesons is challenging because the charm quark mass is not heavy enough to describe exclusive processes with a heavy-quark expansion. The W-annihilation (WA) process may occur as a result of final-state-interactions (FSIs) and the WA amplitude may be comparable with the tree-external-emission amplitude [1–4]. However, the theoretical calculation of the WA amplitude is currently difficult. Hence measurements of decays involving a WA contribution provide the best method to investigate this mechanism.

Among the measured decays involving WA contributions, two decays with VP final states, $D_s^+ \to \omega\pi^+$ and $D_s^+ \to \rho^0\pi^+$, occur only through WA amplitude, and we refer to these as "pure WA decays." Here V and P denote vector and pseudoscalar mesons, respectively. The branching fractions (BFs) of these pure WA decays are at the $\mathcal{O}(0.1\%)$ [5]. These BF measurements allow the determination of two distinct WA amplitudes for VP final states. However, for SP final states, where S denotes a scalar meson, there are neither experimental measurements nor theoretical calculations of the BFs.

Two decays with SP final states $D_s^+ \to a_0(980)^+\pi^0$ and $D_s^+ \to a_0(980)^0\pi^+$ can proceed via the WA transition. If $a_0(980)$ is a $q\bar{q}$ or a tetraquark state, $D_s^+ \to a_0(980)^+\pi^0$ is pure WA decay while $D_s^+ \to a_0(980)^0\pi^+$ further receive contributions from $a_0(980)^0 - f_0(980)$ mixing. Their decay diagrams for the WA process are shown in Fig. 1. In this Letter, we search for them with an amplitude analysis of $D_s^+ \to \pi^+\pi^0\eta$. We also present improved measurements of the BFs of $D_s^+ \to \pi^+\pi^0\eta$ and $D_s^+ \to \rho^+\eta$ decays. Throughout this Letter, charge conjugation and $a_0(980) \to \pi\eta$ are implied unless explicitly stated.

We use a data sample corresponding to an integrated luminosity of 3.19 fb^{-1}, taken at a center-of-mass energy of 4.178 GeV with the BESIII detector located at the Beijing Electron Position Collider [6]. The BESIII detector and the upgraded multigap resistive plate chambers used in the

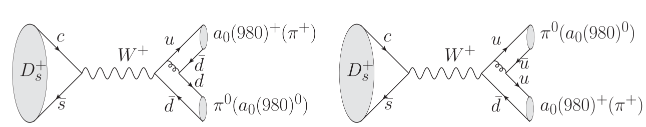

FIG. 1. $D_s^+ \to a_0(980)^{+(0)}\pi^{0(+)}$ WA-topology diagrams, where the gluon lines can be connected with the quark lines in all possible cases and the contributions from FSI are included.

time-of-flight systems are described in Refs. [7] and [8], respectively. We study the background and determine tagging efficiencies with a generic Monte Carlo (GMC) sample that is simulated with GEANT4 [9]. The GMC sample includes all known open-charm decay processes, which are generated with CONEXC [10] and EVTGEN [11], initial-state radiative decays to the J/ψ or $\psi(3686)$, and continuum processes. We determine signal efficiencies from Monte Carlo (MC) samples of $D_s^+ \to \pi^+\pi^0\eta$ decays that are generated according to the amplitude fit results to the data described in this Letter.

In the data sample, the D_s mesons are mainly produced via the process of $e^+e^- \to D_s^{*-}D_s^+$, $D_s^{*-} \to \gamma D_s^-$; we refer to the γ directly produced from the D_s^{*-} decay as $\gamma_{\rm direct}$. To exploit the dominance of the $e^+e^- \to D_s^{*-}D_s^+$ process, we use the double-tag (DT) method [12]. The single-tag (ST) D_s^- mesons are reconstructed using seven hadronic decays: $D_s^- \to K_S^0K^-$, $D_s^- \to K^+K^-\pi^-$, $D_s^- \to K_S^0K^-\pi^0$, $D_s^- \to K^+K^-\pi^-\pi^0$, $D_s^- \to K_S^0K^+\pi^-\pi^-$, $D_s^- \to \pi^-\eta$, and $D_s^- \to \pi^-\eta'$. A DT is formed by selecting a $D_s^+ \to \pi\pi^0\eta$ decay in the side of the event recoiling against the D_s^- tag. Here, K_S^0, π^0, η, and η' are reconstructed using $\pi^+\pi^-$, $\gamma\gamma$, $\gamma\gamma$, and $\pi^+\pi^-\eta$ channels, respectively. The selection criteria for charged tracks, photons, K_S^0, and π^0 are the same as those reported in Ref. [13]. The $\eta^{(\prime)}$ candidate is required to have an invariant mass of the $\gamma\gamma(\pi^+\pi^-\eta)$ combination in the interval $[0.490, 0.580]([0.938, 0.978])$ GeV$/c^2$.

The invariant masses of the tagged (signal) $D_s^{-(+)}$ candidates $M_{\rm tag}(M_{\rm sig})$ without any constraint are required to be in the interval $[1.90, 2.03]$ GeV$/c^2$ ($[1.87, 2.06]$ GeV$/c^2$). For the ST D_s^- mesons, the recoil mass $M_{\rm rec} = [E_{\rm tot} - (|\mathbf{p}_{D_s}|^2 + m_{D_s}^2)^{1/2}]^2 - |\mathbf{p}_{\rm tot} - \mathbf{p}_{D_s}|^2 1/2$ is required to be within the range $[2.05, 2.18]$ GeV$/c^2$ to suppress events from non-$D_s^{*-}D_s^+$ processes. Here, $(E_{\rm tot}, \mathbf{p}_{\rm tot})$ is the four-momentum of the colliding e^+e^- system, $\mathbf{p}_{D_s}$ is the three-momentum of the D_s candidate, and m_{D_s} is the D_s mass [5]. For events with multiple tag candidates for a single tag mode, the one with a value of $M_{\rm rec}$ closest to m_{D_s} is chosen. If there are multiple signal candidates present against a selected tag candidate, the one with a value of $(M_{\rm tag} + M_{\rm sig})/2$ closest to m_{D_s} is accepted.

To successfully perform an amplitude analysis with all events falling within the Dalitz plot and to allow the selection of the $\gamma_{\rm direct}$ candidate, we perform a seven-constraint (7C) kinematic fit, where aside from constraints arising from four-momentum conservation, the invariant masses of the $(\gamma\gamma)_{\pi^0}$, $(\gamma\gamma)_\eta$, and $\pi^+\pi^0\eta$ combinations used to reconstruct the signal D_s^+ candidate are constrained to the nominal π^0, η and D_s^+ masses [5], respectively. The $\gamma_{\rm direct}$ candidate used in the 7C fit that produces the smallest $\chi^2_{7\rm C}$ is selected. We only require the kinematic fit to be successful to avoid introducing a broad peak in the background distribution of $M_{\rm sig}$ arising from events that are inconsistent with the signal hypothesis. Then, we perform another 7C kinematic fit, referred to as the "7CA fit," by replacing the signal D_s^+ mass constraint with a D_s^* mass constraint in which the invariant mass of either the D_s^+ or D_s^- candidate and the selected $\gamma_{\rm direct}$ is constrained to the nominal D_s^* mass [5]. To ensure reasonable consistency with the signal hypothesis, the hypothesis with smaller 7CA χ^2 is selected. To suppress the background associated with the fake $\gamma_{\rm direct}$ candidates in the signal events, we veto events with $\cos\theta_\eta < 0.998$, where θ_η is the angle between the η momentum vector from a η mass constraint fit and that from the 7CA kinematic fit. After applying these criteria, we further reduce the background, by using a multivariable analysis method [14] in which a boosted decision tree (BDT) classifier is developed using the GMC sample. The BDT takes three discriminating variables as inputs: the invariant mass of the photon pair used to reconstruct the η candidate, the momentum of the lower-energy photon from the η candidate, and the momentum of the $\gamma_{\rm direct}$ candidate. Studies of the GMC sample show that a requirement on the output of the BDT retains 77.8% signal and rejects 73.4% background. Events in which the signal candidate lies within the interval $1.93 < M_{\rm sig} < 1.99$ GeV$/c^2$ are retained for the amplitude analysis. The background events in the signal region from the GMC sample are used to model the corresponding background in the data. To check the validity of the GMC background modeling, we compare the $M_{\pi^-\pi^0}$, $M_{\pi^+\eta}$, and $M_{\pi^0\eta}$ distributions of events outside the selected $M_{\rm sig}$ interval between the data and the GMC sample; the distributions are found to be compatible within the statistical uncertainties. We retain a sample of 1239 $D_s^+ \to \pi^+\pi^-\eta$ candidates that has a purity of $(97.7 \pm 0.5)\%$.

The amplitude analysis is performed using an unbinned maximum-likelihood fit to the accepted candidate events in the data. The background contribution is subtracted in the likelihood calculation by assigning negative weights to the background events. The total amplitude $\mathcal{M}(p_j)$ is modeled as the coherent sum of the amplitudes of all intermediate processes, $\mathcal{M}(p_j) = \sum c_n e^{i\phi_n} A_n(p_j)$, where c_n and ϕ_n are the magnitude and phase of the nth amplitude, respectively. The nth amplitude $A_n(p_j)$ is given by $A_n(p_j) = P_n S_n F_n^r F_n^D$. Here P_n is a function that describes the propagator of the intermediate resonance. The resonance ρ^+ is parametrized by a relativistic Breit-Wigner function, while the resonance $a_0(980)$ is parametrized as a two-channel-coupled Flatté formula ($\pi\eta$ and $K\bar{K}$), $P_{a_0(980)} = 1/[(m_0^2 - s_a) - i(g_{\eta\pi}^2\rho_{\eta\pi} + g_{K\bar{K}}^2\rho_{K\bar{K}})]$. Here, $\rho_{\eta\pi}$ and $\rho_{K\bar{K}}$ are the phase space factors: $2q/\sqrt{s_a}$, where q is denoted as the magnitude of the momentum of the daughter particle in the rest system and s_a is the invariant mass squared of $a_0(980)$. We use the coupling constants $g_{\eta\pi}^2 = 0.341 \pm 0.004$ GeV$^2/c^4$ and $g_{K\bar{K}}^2 = (0.892 \pm 0.022) g_{\eta\pi}^2$, reported in Ref. [15]. The function S_n describes angular-momentum conservation in the decay and is constructed using the covariant tensor formalism [16]. The function $F_n^{r(D)}$ is the Blatt-Weisskopf barrier factor of the intermediate state (D_s meson). To quantify the relative contribution of the nth intermediate process, the fit fraction (FF) is calculated with $\mathrm{FF}_n = \int |A_n|^2 d\Phi_3 / \int |\mathcal{M}|^2 d\Phi_3$, where $d\Phi_3$ is the standard element of the three-body phase space. Furthermore, according to the topology diagrams shown in Fig. 1, the W-annihilation amplitudes of the decays $D_s^+ \to a_0(980)^+\pi^0$ and $D_s^+ \to a_0(980)^0\pi^+$ imply the relationship $A(D_s^+ \to a_0(980)^+\pi^0) = -A(D_s^+ \to a_0(980)^0\pi^+)$.

For each amplitude, the statistical significance is determined from the change in log-likelihood and the number of degrees of freedom (NDOF) when the fit is performed with and without the amplitude included. In the nominal fit, only amplitudes that have a significance greater than 5σ are considered, where σ is the standard deviation. In addition to the $D_s^+ \to \rho^+\eta$ amplitude, both $D_s^+ \to a_0(980)^+\pi^0$ and $D_s^+ \to a_0(980)^0\pi^+$ amplitudes are found to be significant. In the fit, however, we notice that the latter two amplitudes have highly correlated phases; their c_n's are consistent with each other and the difference in ϕ_n is found to be close to π. The given FF of $D_s^+ \to a_0(980)^0\pi^+$ is greater than the expected $a_0(980)^0 - f_0(980)$ mixing effect [17] by 2 orders of magnitude. Consequently, in the nominal fit, we neglect the $a_0(980)^0 - f_0(980)$ mixing effect and set the values of c_n of these two amplitudes to be equal with a phase difference of π. We refer to the coherent sum of these two amplitudes as "$D_s^+ \to a_0(980)\pi$." The nonresonant process $D_s^+ \to (\pi^+\pi^0)_V\eta$ is also considered, where the subscript V denotes a vector nonresonant state of the $\pi^+\pi^0$ combination. We consider other possible amplitudes that involve $\rho(1450)$, $a_0(1450)$, $\pi_1(1400)$, $a_2(1320)$, or $a_2(1700)$, as well as the nonresonant partners; none of these amplitudes has a statistical significance greater than 2σ, so they are not included in the nominal model. In the fit, the values of c_n and ϕ_n for the $D_s^+ \to \rho^+\eta$ amplitude are fixed to be one and zero, respectively, so that all other amplitudes are measured relative to this amplitude. The masses and widths of the intermediate resonances used in the fit, except for those of the $a_0(980)$, are taken from Ref. [5].

For $D_s^+ \to \rho^+\eta$, $D_s^+ \to (\pi^+\pi^0)_V\eta$, and $D_s^+ \to a_0(980)\pi$, the resulting statistical significances are greater than 20σ, 5.7σ, and 16.2σ, respectively. Their phases and FFs are listed in Table I. The Dalitz plot of $M^2_{\pi^+\eta}$ vs $M^2_{\pi^0\eta}$ for the data is

TABLE I. Significance, ϕ_n, and FF_n for the intermediate processes in the nominal fit. The first and second uncertainties are statistical and systematic, respectively.

Amplitude	ϕ_n (rad)	FF_n
$D_s^+ \to \rho^+\eta$	0.0 (fixed)	$0.783 \pm 0.050 \pm 0.021$
$D_s^+ \to (\pi^+\pi^0)_V\eta$	$0.612 \pm 0.172 \pm 0.342$	$0.054 \pm 0.021 \pm 0.025$
$D_s^+ \to a_0(980)\pi$	$2.794 \pm 0.087 \pm 0.044$	$0.232 \pm 0.023 \pm 0.033$

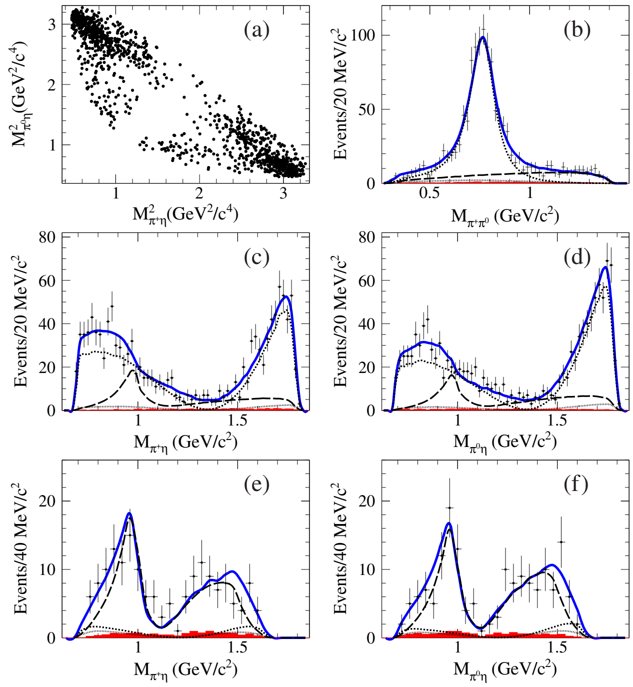

FIG. 2. (a) Dalitz plot of $M^2_{\pi^+\eta}$ vs $M^2_{\pi^0\eta}$ for data, the projections of the fit on (b) $M_{\pi^-\pi^0}$, (c) $M_{\pi^+\eta}$, and (d) $M_{\pi^0\eta}$, and the projections on (e) $M_{\pi^+\eta}$ and (f) $M_{\pi^0\eta}$ after requiring $M_{\pi^+\pi^0} > 1.0\ \mathrm{GeV}/c^2$. In (b)–(f), the dots with error bars and the solid line are data and the total fit, respectively; the dashed, dotted, and long-dashed lines are the contributions from $D_s^+ \to \rho^+\eta$, $D_s^+ \to (\pi^+\pi^0)_V\eta$, and $D_s^+ \to a_0(980)\pi$, respectively. The (red) hatched histograms are the simulated background.

shown in Fig. 2(a). The projections of the fit on $M_{\pi^-\pi^0}$, $M_{\pi^+\eta}$, and $M_{\pi^0\eta}$ are shown in Figs. 2(b)–2(d). The projections on $M_{\pi^+\eta}$ and $M_{\pi^0\eta}$ for events with $M_{\pi^+\pi^0} > 1.0\ \mathrm{GeV}/c^2$ are shown in Figs. 2(e) and 2(f), in which $a_0(980)$ peaks are observed. The fit quality is determined by calculating the χ^2 of the fit using an adaptive binning of the $M^2_{\pi^+\eta}$ vs $M^2_{\pi^0\eta}$ Dalitz plot that requires each bin contains at least 10 events. The goodness of fit is $\chi^2/\mathrm{NDOF} = 82.8/77$.

Systematic uncertainties for the amplitude analysis are considered from five sources: (I) line shape parameterizations of the resonances, (II) fixed parameters in the amplitudes, (III) the background level and distribution in the Dalitz plot, (IV) experimental effects, and (V) the fitter performance. We determine these systematic uncertainties separately by taking the difference between the values of ϕ_n, and FF_n found by the altered and nominal fits. The uncertainties related to the assumed resonance line shape are estimated by using the following alternatives: a Gounaris-Sakurai function [21] for the ρ^+ propagator and a three-channel-coupled Flatté formula, which adds the $\pi\eta'$ channel [15], for the $a_0(980)$ propagator. Since varying the propagators results in different normalization factors, the effect on all FFs is considered. The uncertainties related to the fixed parameters in the amplitudes are considered by varying the mass and width of ρ^+ by $\pm 1\sigma$ [5], the mass and coupling constants of $a_0(980)$ by the uncertainties reported in Ref. [15], and the effect of varying the radii of the nonresonant state and D_s meson within ± 2 GeV^{-1}. In addition, for the ρ^+ resonance, the effective radius reported in Ref. [5] is used as an alternative. The uncertainty related to the assumed background level is determined by changing the background fraction within its statistical uncertainty. The uncertainty related to the assumed background shape is estimated by using an alternative distribution simulated with $D_s^+ \to \pi^+ f_0(980)$, $f_0(980) \to \pi^0\pi^0$. To estimate the uncertainty from the experimental effect related to the kinematic fits and BDT classifier, we alter the χ^2 requirements for the result of the two kinematic fits, the $\cos\theta_\eta$ requirement, and the BDT requirement such that the purity is approximately equal to the sample used in the nominal fit. The fitter performance is investigated with the same method as reported in Ref. [22]. The biases are small and taken as the systematic uncertainties. The contributions of individual systematic uncertainties are summarized in Table II, and are added in quadrature to obtain the total systematic uncertainty.

Further, we measure the total BF of $D_s^+ \to \pi^+\pi^0\eta$ without reconstructing $\gamma_{\rm direct}$ to improve the statistical precision. The ST yields ($Y_{\rm tag}$) and DT yield ($Y_{\rm sig}$) of data are determined by the fits to the resulting $M_{\rm tag}$ and $M_{\rm sig}$ distributions, as shown in Figs. 3(a)–3(g) and Fig. 3(h), respectively. In each fit, the signal shape is modeled with the MC-simulated shape convoluted with a Gaussian function, which accounts for any difference in resolution between data and MC calculations, and the background is described with a second-order Chebychev polynomial. These fits give a total ST yield of $Y_{\rm tag} = 255895 \pm 1358$ and a signal yield of $Y_{\rm sig} = 2626 \pm 77$. Based on the signal MC sample, generated according to the amplitude analysis results reported in this Letter, the DT efficiencies ($\epsilon_{\rm tag,sig}$) are determined. With $Y_{\rm tag}$, $Y_{\rm sig}$, $\epsilon_{\rm tag,sig}$, and the ST efficiencies ($\epsilon_{\rm tag}$), the relationship $\mathcal{B}(D_s^+ \to \pi^+\pi^0\eta) = (Y_{\rm sig}/\sum_i Y^i_{\rm tag}\epsilon^i_{\rm tag,sig}/\epsilon^i_{\rm tag})$, where the index i denotes the ith tag mode, is used to obtain $\mathcal{B}(D_s^+ \to \pi^+\pi^0\eta) = (9.50 \pm 0.28_{\rm stat})\%$.

TABLE II. Systematic uncertainties on the ϕ and FFs for different amplitudes, in units of the corresponding statistical uncertainties.

Amplitude		Source I	II	III	IV	V	Total
$D_s^+ \to \rho^+\eta$	FF	0.06	0.34	0.13	0.12	0.15	0.41
$D_s^+ \to (\pi^+\pi^0)_V\eta$	ϕ	$\cdots$	1.97	0.18	0.03	0.17	1.99
	FF	0.61	1.03	0.12	0.06	0.08	1.21
$D_s^+ \to a_0(980)\pi$	ϕ	$\cdots$	0.41	0.07	0.28	0.09	0.51
	FF	0.58	1.31	0.02	0.06	0.11	1.45

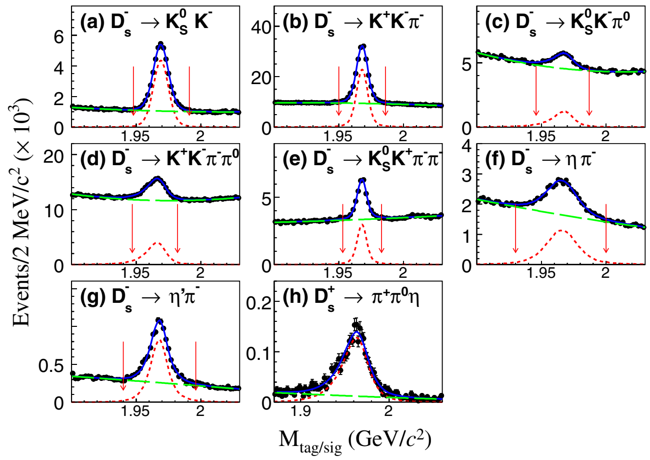

FIG. 3. Fits to (a)–(g) the $M_{\rm tag}$ distributions of seven tag modes (indicated in each sub-figure) and (h) the $M_{\rm sig}$ distribution of signal candidates. The dots with error bars are data. The (blue) solid lines are the total fit. The (red) dashed and the (green) long-dashed lines are signal and background, respectively. In (a)–(g), the D_s^- signal regions are between the arrows.

For the total BF measurement, the systematic uncertainty related to the signal shape is studied by performing an alternative fit without convolving the Gaussian resolution function. The BF shift of 0.5% is taken as the uncertainty. The systematic uncertainty arising from the assumed background shape and the fit range is studied by replacing our nominal ones with a first-order Chebychev polynomial and a fit range of $[1.88, 2.04]$ GeV$/c^2$, respectively. The largest BF shift of 0.6% is taken as the related uncertainty. The possible bias due to the measurement method is estimated to be 0.2% by comparing the measured BF in the GMC sample, using the same method as in data analysis, to the value assumed in the generation. The uncertainties from particle identification and tracking efficiencies are assigned to be 0.5% and 1.0% [13], respectively. The relative uncertainty in the π^0 reconstruction efficiency is 2.0% [13], and the uncertainty in η reconstruction is assumed to be comparable to that on π^0 reconstruction and correlated with it. The uncertainty from the Dalitz model of 0.6% is estimated as the change of efficiency when the model parameters are varied by their systematic uncertainties (this term is not considered when calculating the BFs of the intermediate processes). The uncertainties due to MC statistics (0.2%) and the value of $\mathcal{B}(\pi^0/\eta \to \gamma\gamma)$ used [5] (0.5%) are also considered. Adding these uncertainties in quadrature gives a total systematic uncertainty of 4.3%.

We obtain $\mathcal{B}(D_s^+ \to \pi^+\pi^0\eta)$ to be $(9.50 \pm 0.28_{\rm stat} \pm 0.41_{\rm sys})\%$. Using the FFs listed in Table I, the BFs for the intermediate processes $D_s^+ \to \rho^+\eta$ and $D_s^+ \to (\pi^+\pi^0)_V\eta$ are calculated to be $(7.44 \pm 0.52_{\rm stat} \pm 0.38_{\rm sys})\%$ and $(0.51 \pm 0.20_{\rm stat} \pm 0.25_{\rm sys})\%$, respectively. With the definition of the fit fraction, the fraction of $D_s^+ \to a_0(980)^{+(0)}\pi^{0(+)}$,

$a_0(980)^{+(0)} \to \pi^{+(0)}\eta$ with respect to the total fraction of $D_s^+ \to a_0(980)\pi, a_0(980) \to \pi\eta$ is evaluated to be 0.66. Multiplying by the FF of $D_s^+ \to a_0(980)\pi$ determined from the nominal fit and $\mathcal{B}(D_s^+ \to \pi^+\pi^0\eta)$, the BF of $D_s^+ \to a_0(980)^{+(0)}\pi^{0(+)}, a_0(980)^{+(0)} \to \pi^{+(0)}\eta$ is determined to be $(1.46 \pm 0.15_{\rm stat} \pm 0.23_{\rm sys})\%$.

In summary, we present the first amplitude analysis of the decay $D_s^+ \to \pi^+\pi^0\eta$. The absolute BF of $D_s^+ \to \pi^+\pi^0\eta$ is measured with a precision improved by a factor of 2.5 compared with the world average value [5]. We observe the pure WA decays $D_s^+ \to a_0(980)\pi$ for the first time with a statistical significance of 16.2σ. The measured $\mathcal{B}(D_s^+ \to a_0(980)^{+(0)}\pi^{0(+)})$ is larger than other measured BFs of pure WA decays $D_s^+ \to \omega\pi^+$ and $D_s^+ \to \rho^0\pi^+$ by at least one order of magnitude. Furthermore, when the measured $a_0(980)^0$-$f_0(980)$ mixing rate [18] is considered, the expected effect of $a_0(980)^0$-$f_0(980)$ mixing is lower than the WA contribution in $D_s^+ \to a_0(980)^0\pi^+$ decay by 2 orders of magnitude, make it negligible in this measurement.

With the measured $\mathcal{B}(D_s^+ \to a_0(980)^{+(0)}\pi^{0(+)})$, the WA contribution with respect to the tree-external-emission contribution in SP mode is estimated to be 0.84 ± 0.23 [23], which is significantly greater than that (0.1–0.2) in VP and PP modes [3,4]. This measurement sheds light on the FSI effect and nonperturbative effects of the strong interaction [1,4], and provides a theoretical challenge to understanding such a large WA contribution. In addition, the result of this analysis is an essential input to determine the effect from $a_0(980)^0$ on the K^+K^- S-wave contribution to the model-dependent amplitude analysis of $D_s^+ \to K^+K^-\pi^+$ [24,25].

The authors greatly thank Professor Fu-Sheng Yu and Professor Haiyang Cheng for the useful discussions. The BESIII Collaboration thanks the staff of BEPCII and the IHEP computing center for their strong support. This work is supported in part by National Key Basic Research Program of China under Contract No. 2015CB856700; National Natural Science Foundation of China (NSFC) under Contracts No. 11475185, No. 11625523, No. 11635010, No. 11735014; the Chinese Academy of Sciences (CAS) Large-Scale Scientific Facility Program; the CAS Center for Excellence in Particle Physics (CCEPP); Joint Large-Scale Scientific Facility Funds of the NSFC and CAS under Contracts No. U1332201, No. U1532257, No. U1532258; CAS Key Research Program of Frontier Sciences under Contracts No. QYZDJ-SSW-SLH003, No. QYZDJ-SSW-SLH040; 100 Talents Program of CAS; National 1000 Talents Program of China; INPAC and Shanghai Key Laboratory for Particle Physics and Cosmology; German Research Foundation DFG under Contracts No. Collaborative Research Center CRC 1044, FOR 2359; Istituto Nazionale di Fisica Nucleare, Italy; Koninklijke Nederlandse Akademie van Wetenschappen (KNAW) under Contract No. 530-4CDP03; Ministry of Development of Turkey under Contract No. DPT2006K-120470; National Science and Technology fund; The Swedish Research Council; U.S. Department of Energy under Contracts No. DE-FG02-05ER41374, No. DE-SC-0010118, No. DE-SC-0010504, No. DE-SC-0012069; University of Groningen (RuG) and the Helmholtzzentrum fuer Schwerionenforschung GmbH (GSI), Darmstadt; WCU Program of National Research Foundation of Korea under Contract No. R32-2008-000-10155-0.

[*]Corresponding author.
luy@ihep.ac.cn
[a]Also at Bogazici University, 34342 Istanbul, Turkey.
[b]Also at the Moscow Institute of Physics and Technology, Moscow 141700, Russia.
[c]Also at the Functional Electronics Laboratory, Tomsk State University, Tomsk 634050, Russia.
[d]Also at the Novosibirsk State University, Novosibirsk 630090, Russia.
[e]Also at the NRC "Kurchatov Institute," PNPI, 188300 Gatchina, Russia.
[f]Also at Istanbul Arel University, 34295 Istanbul, Turkey.
[g]Also at Goethe University Frankfurt, 60323 Frankfurt am Main, Germany.
[h]Also at Key Laboratory for Particle Physics, Astrophysics and Cosmology, Ministry of Education; Shanghai Key Laboratory for Particle Physics and Cosmology; Institute of Nuclear and Particle Physics, Shanghai 200240, People's Republic of China.
[i]Government College Women University, Sialkot 51310, Punjab, Pakistan.
[j]Key Laboratory of Nuclear Physics and Ion-beam Application (MOE) and Institute of Modern Physics, Fudan University, Shanghai 200443, People's Republic of China.
[k]Present address: Center for Underground Physics, Institute for Basic Science, Daejeon 34126, Korea.
[l]Also at Shanxi Normal University, Linfen 041004, People's Republic of China.

[1] H. Y. Cheng and C. W. Chiang, Phys. Rev. D **81**, 074021 (2010).
[2] H. N. Li, C. D. Lu, and F. S. Yu, Phys. Rev. D **86**, 036012 (2012).
[3] Q. Qin, H. N. Li, C. D. Lu, and F. S. Yu, Phys. Rev. D **89**, 054006 (2014).
[4] H. Y. Cheng, C. W. Chiang, and A. L. Kuo, Phys. Rev. D **93**, 114010 (2016).
[5] M. Tanabashi *et al.* (Particle Data Group), Phys. Rev. D **98**, 030001 (2018).
[6] C. H. Yu *et al.*, Proceeding of IPAC2016, Busan, Korea, 2016.
[7] M. Ablikim *et al.* (BESIII Collaboration), Nucl. Instrum. Methods Phys. Res., Sect. A **614**, 345 (2010).
[8] X. Wang *et al.*, J. Instrum. **11**, C08009 (2016).
[9] S. Agostinelli *et al.* (GEANT4 Collaboration), Nucl. Instrum. Methods Phys. Res., Sect. A **506**, 250 (2003).
[10] R. G. Ping, Chin. Phys. C **38**, 083001 (2014).
[11] D. J. Lange, Nucl. Instrum. Methods Phys. Res., Sect. A **462**, 152 (2001); R. G. Ping, Chin. Phys. C **32**, 243 (2008).

[12] R. M. Baltrusaitis *et al.* (Mark III Collaboration), Phys. Rev. Lett. **56**, 2140 (1986).

[13] M. Ablikim *et al.* (BESIII Collaboration), Phys. Rev. D **99**, 091101 (2019).

[14] A. Hocker *et al.*, Proc. Sci. ACAT2007 (**2007**) 040.

[15] M. Ablikim *et al.* (BESIII Collaboration), Phys. Rev. D **95**, 032002 (2017).

[16] B. S. Zou and D. V. Bugg, Eur. Phys. J. A **16**, 537 (2003).

[17] The size of $a_0(980)^0$-$f_0(980)$ mixing contribution is estimated to be $\mathcal{O}(0.01\%)$ with the $\mathcal{B}(D_s^+ \to f_0\pi^+)$ and the measured $a_0(980)^0 - f_0(980)$ mixing rate [18], where $\mathcal{B}(D_s^+ \to f_0\pi^+)$ is evaluated with $\mathcal{B}(D_s^+ \to f_0\pi^+) = \mathcal{B}(D_s^+ \to f_0\pi^+, f_0 \to \pi\pi)(1 + r_{f_0})$. Here, $\mathcal{B}(D_s^+ \to f_0\pi^+, f_0 \to \pi\pi)$ is obtained from Ref. [19] and PDG. The ratio r_{f_0} is given by Ref. [20].

[18] M. Ablikim *et al.* (BESIII Collaboration), Phys. Rev. Lett. **121**, 022001 (2018).

[19] E. M. Aitala *et al.* (E791 Collaboration), Phys. Rev. Lett. **86**, 765 (2001).

[20] M. Ablikim *et al.* (BES Collaboration), Phys. Rev. D **72**, 092002 (2005).

[21] G. J. Gounaris and J. J. Sakurai, Phys. Rev. Lett. **21**, 244 (1968).

[22] M. Ablikim *et al.* (BESIII Collaboration), Phys. Rev. D **95**, 072010 (2017).

[23] 0.84 ± 0.23 is obtained with $\sqrt{\frac{\mathcal{B}(D_s^+ \to a_0(980)^+\pi^0)(1+r_{a_0})}{2\mathcal{B}(D_s^+ \to f_0(980)\pi^+)}}$ $(1+r_{f_0})$, where, in the denominator, $f_0(980) \to \pi\pi$ and $r_{a_0} = \frac{\Gamma(a_0(980)\to K\bar{K})}{\Gamma(a_0(980)\to \eta\pi)}$. The ratio of r_{a_0} is given by PDG.

[24] R. E. Mitchell *et al.* (CLEO Collaboration), Phys. Rev. D **79**, 072008 (2009).

[25] P. del Amo Sanchez *et al.* (*BABAR* Collaboration), Phys. Rev. D **83**, 052001 (2011).